

Article

Performance Study of Methane Dry Reforming on Ni/ZrO₂ Catalyst

Anis H. Fakeeha , Abdulrahman Kurdi, Yousef A. Al-Baqmaa , Ahmed A. Ibrahim * , Ahmed E. Abasaed 
and Ahmed S. Al-Fatesh * 

Department of Chemical Engineering, College of Engineering, King Saud University, P.O. Box 800, Riyadh 11421, Saudi Arabia; anishf@ksu.edu.sa (A.H.F.); abdulkurdi@gmail.com (A.K.); yousef201629@gmail.com (Y.A.A.-B.); abasaed@ksu.edu.sa (A.E.A.)

* Correspondence: aidid@ksu.edu.sa (A.A.I.); aalfatesh@ksu.edu.sa (A.S.A.-F.)

Abstract: Dry reforming of methane (DRM) has important and positive environmental and industrial impacts, as it consumes two of the top greenhouse gases in order to produce syngas (H₂ and CO) and thus hydrogen (H₂). The performance of DRM of conversions of CH₄ and CO₂ was investigated over Ni/ZrO₂ catalysts. The catalytic performance of all prepared catalysts for DRM was assessed in a micro-tubular fixed bed reactor under similar reaction conditions (i.e., activation and reaction temperatures at 700 °C, a feed flow rate of 70 mL/min, reaction temperature, and a 440 min reaction time). Various characterization techniques, such as BET, CO₂-TPD, TGA, XRD, EDX, and TEM, were employed. The zirconia support was modified with MgO or Y₂O₃. The yttria-stabilized zirconia catalyst (5Ni15YZr) provided the optimum activity performance of CH₄ and CO₂ conversions of 56.1 and 64.3%, respectively, at 700 °C and a 70 mL/min flow rate; this catalyst also had the highest basicity. The Ni-based catalyst was promoted with Cs, Ga, and Sr. The Sr-promoted catalyst produced the highest enhancement of activity. The influence of the reaction temperature and the feed flow rate on 5Ni15YZr and 5NiSr15YZr indicated that the activity increased with the increase in the reaction temperature and lower feed flow rate. For 5Ni3Sr15YZr, at a reaction temperature of 800 °C, the CH₄ and CO₂ conversions were 76.3 and 79.9%, respectively, whereas at 700 °C, the conversions of CH₄ and CO₂ were 66.6 and 79.6% respectively.

Keywords: dry reforming of CH₄; greenhouse gases; nickel; synthesis gas; ZrO₂



Citation: Fakeeha, A.H.; Kurdi, A.; Al-Baqmaa, Y.A.; Ibrahim, A.A.; Abasaed, A.E.; Al-Fatesh, A.S. Performance Study of Methane Dry Reforming on Ni/ZrO₂ Catalyst. *Energies* **2022**, *15*, 3841. <https://doi.org/10.3390/en15103841>

Academic Editors: Devinder Mahajan and Diego Luna

Received: 15 April 2022

Accepted: 19 May 2022

Published: 23 May 2022

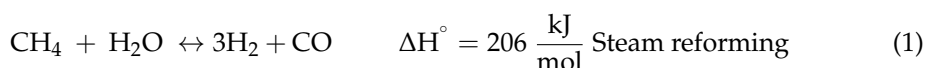
Publisher's Note: MDPI stays neutral with regard to jurisdictional claims in published maps and institutional affiliations.

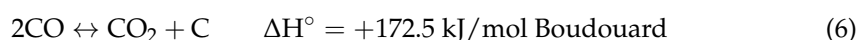
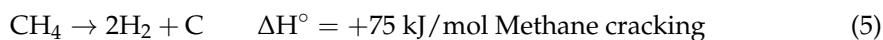
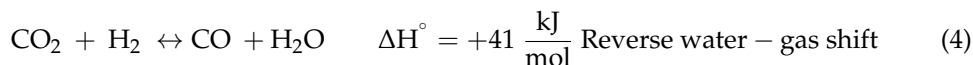
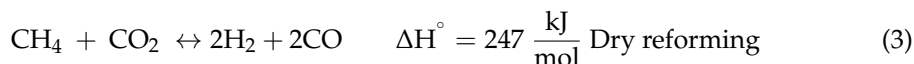
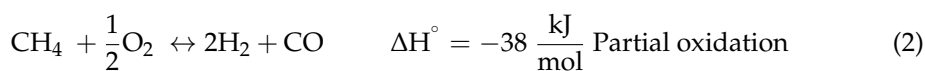


Copyright: © 2022 by the authors. Licensee MDPI, Basel, Switzerland. This article is an open access article distributed under the terms and conditions of the Creative Commons Attribution (CC BY) license (<https://creativecommons.org/licenses/by/4.0/>).

1. Introduction

Currently, greenhouse gases (chiefly CO₂ and CH₄), which can lead to global warming and energy shortages, are major challenges for the world. It is shocking that the CO₂ composition in the atmosphere has reached the level of 400 ppm, which has elevated the temperature of the earth by 1.5 °C [1]. The potentiality of methane to cause global warming is 25 times higher than that of CO₂ [2]. Thus, it is necessary to come up with a strategy that alleviates the carbon footprint of contemporary civilizations and tackles these challenges. Dry reforming of methane (DRM) is regarded among the existing strategies owing to its ability to consume CO₂ and CH₄ so as to generate syngas (CO+H₂), an environmentally safe and cheap product [3–5]. At present, large-scale technologies for manufacturing syngas have been performed. The emerging industrial processes comprise lab-scale studies of DRM, partial oxidation, and methane steam reforming [6]. Compounds such as those produced by hydroformylation are directly manufactured from syngas. The H₂/CO ratio can be attuned to producing dimethyl ether, methanol, oil, or fuel via the Fischer–Tropsch process. DRM is usually accompanied by a reverse water–gas shift reaction.





Noble metals have good performance in the reforming process; however, they are ruled out because of their scarcity and high cost [7]. Transition metals, such as Ni and Co, are universally considered to be suitable catalysts for DRM because of their low cost, but deactivation due to carbon deposition hampers the industrial application of the process. The stability and activity can be enhanced by the use of proper support. Mourhly et al. used mesoporous silica as support for Ni-based catalysts in DRM [8]. The results showed that the catalysts exhibited long-term stability with low coke formation predominantly as carbon nanotubes. Arif et al. [9] employed Ni/ZrO₂ and Ni/CaO catalysts to generate H₂ through CO₂ reforming of glycerol. The performance and activity of the catalysts usually depend on several factors, which include the diameter, support type, promoters, acid–base features, and oxidation numbers of the metals [10]. For Ni particles to be used as catalysts for DRM at 500 to 600 °C and 5.0 bar, the most effective size is around 2–3 nm [11]. Computational performance studies using a single-site Ni/MgO catalyst in DRM revealed that the binding between the Ni and MgO had too low of a synergistic effect because of the limited number of active sites. However, increasing the Ni over the MgO enhanced the binding and promoted the removal of carbon [12]. Al-Fatesh et al. investigated the DRM using an Ni catalyst supported by a combination of La₂O₃ and ZrO₂ [13]. It was found that the Ni dispersion over the lanthana–zirconia support stabilized the tetragonal ZrO₂ phase. The support had additional amorphous La₂O₂CO₃ species and format species, which indicated a broad interaction of CO₂ over the catalyst surface. Numerous studies have evaluated the function of support in the performance of Ni catalysts. For instance, Ni/ZnAl₂O₄ exhibited the highest resistance to carbon deposition and metal sintering. Supports of alumina and silica oxidize Ni during the process, while ZrO₂ stabilizes Ni particles, thus increasing the efficiency of methane conversion into fuel. The stability is due to the water accumulation behavior of ZrO₂, which favors the formation of hydroxyl for the greater efficacy of SRM and DRM. CeO₂ and ZrO₂ are ideal supports for Ni catalysts in DRM because of their high storage capacity of oxygen, great resistance to coking, and redox properties. These features give superior catalytic properties compared with the conventional supports used so far, such as aluminum oxide and MgAl₂O₃. Doping Ni with other metals as promoters improves the activity, efficiency, stability, and durability of the catalysts. As a model, the combination of Ni with Fe to form the alloy Ni-Fe showed a methane conversion of 97.5% and exhibited selectivity of 92.9% for carbon monoxide at a temperature of 900 °C [14]. Wysocka and colleagues examined the impact of a K promoter on Ni-based catalysts for DRM [15]. Their results revealed that K promotion of nickel altered the nickel distribution and metal–support interactions and decelerated carbon deposition while enhancing the sorption of carbon dioxide. Abd Ghani et al. found that Nb promoters improved the catalytic activity of the Ni-based catalyst because of the improvement in the morphology and the electronic adjustment of the catalyst [16]. The Nb promoter increased CO₂ conversion. This study aims to assess the performance activities in DRM with Ni/ZrO₂ catalysts, including aspects of the support modifiers MgO and Y₂O₃; different loading of the best modifiers; the effects of Sc, Ga, and Sr promoters; and, finally, the sensitivity test of the optimum non-promoted catalyst in terms the temperature and flow rate. Relevant characterization methods were performed to better comprehend the different features of the catalytic system.

2. Materials and Methods

Nitrate of Ni, Ga, Cs, and Sr: $[\text{Ni}(\text{NO}_3)_2 \cdot 6\text{H}_2\text{O}]$, $[\text{Ga}(\text{NO}_3)_3 \cdot 6\text{H}_2\text{O}]$, $[\text{CsNO}_3]$, and $[\text{Sr}(\text{NO}_3)_2 \cdot 4\text{H}_2\text{O}]$ with 99% purity was acquired from Sigma-Aldrich (Haverhill, MA, USA). Anhui Elite industrial provided the zirconia (ZrO_2) support with 99% purity. Yttria (Y_2O_3 , 99.9%) was purchased from Canada, and MgO (99.9%) was bought from Sigma-Aldrich. In the impregnation process, pure H_2O was employed. The summary of catalyst synthesis, activity, and characterization are provided in the Supplementary Materials. The prepared catalysts along with their compositions and denotations are shown in Table S1.

3. Results

For verification of the performed preparations, a sample (5Ni10YZr) was tested using EDX characterization; in Figure S1, the images display the peaks for O_2 , Ni, Y, and Zr, and therefore, the elemental analysis was found to be consistent with the compositions of the tested catalyst. The quantity aspects of the elements closely resembled those of the given sample. Zirconium dioxide has three crystalline phases: a monoclinic phase below 1170°C , a tetragonal phase between 1170°C and 2370°C , and a cubic phase above 2370°C [17,18]. ZrO_2 exhibits thermal stability, oxygen vacancies, and electrical conductivity, and its properties can be improved by adding cations of lanthanide and alkaline earth, such as Mg^{2+} , Ca^{2+} , La^{3+} , or Y^{3+} , into the ZrO_2 lattice because it has a lower valence than Zr^{4+} , leading to an overall negative charge [19]. As shown in Figure 1, the 5Ni5YZr catalyst improved the conversion of methane and carbon dioxide. While the 5Ni5MgZr reduced the activity performance with respect to pristine catalyst (5NiZr), the CH_4 and CO_2 conversions decreased in the order $5\text{Ni}5\text{YZr} > 5\text{NiZr} > 5\text{Ni}5\text{MgZr}$. The observed variations of activities with the addition of Mg and Y could be related to the metal support interactions, which, in the case of Y, led to a decrease in CH_4 and CO_2 activation energies and hence promoted the conversions. By contrast, in Mg, the opposite phenomenon was observed, in which the metal and the modified support interactions increased the energy activations of CH_4 and CO_2 , and the reactivity thus decreased.

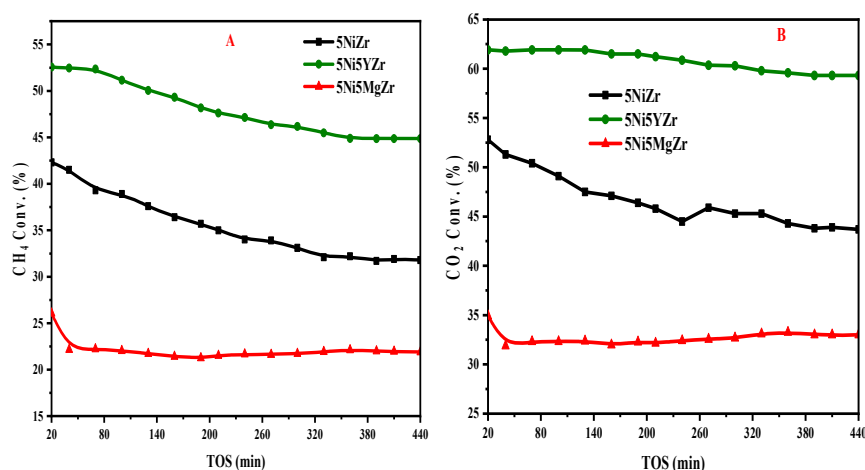


Figure 1. (A) CH_4 conversion %; (B) CO_2 conversion % against time on stream (TOS) for the potential modifiers at a reaction temperature of 700°C .

Recent studies have shown the impact of yttrium oxide (Y_2O_3) on the stabilization of ZrO_2 [20]. To determine the optimum Y_2O_3 loading, five different wt.% loading conditions ($x = 0.0, 5.0, 10.0, 15.0,$ and 20.0 wt.%) were applied to synthesize the $5\text{Ni}x\text{YZr}$. The essential features of the fresh catalysts were examined using nitrogen adsorption–desorption isotherms. Figure S2 displays the outcomes of the isotherms. According to the IUPAC sorting of isotherms, the isotherms fell under the classification of type V, with an H1-type hysteresis loop that resulted from the evaporation at high relative pressures and the capillary condensation [21]. The relative pressure (P/P_0) augmented in the span of 0.80 – 1.00 .

In addition, the low specific surface areas of all catalysts resulted from the low specific volume N_2 adsorbed, occurring in the extent of 4.5–8.0 cm^3/g . Table 1 outlines the textural properties. The pristine ZrO_2 displayed a BET value of 21.0 m^2/g , which diminished to 16.0 m^2/g when NiO was impregnated, an indication of proper loading. Nevertheless, the pore size expanded from 37.0 nm for meso- ZrO_2 to 42.0 nm after NiO impregnation because of the evolution of H_2O , NO_2 , HNO_3 , and O_2 gases and the decomposition of nickel (II) nitrate hexahydrate [22] throughout the course of the calcination stages. The BET value of the catalysts increased when Y_2O_3 was put in, and this was related to a reduction in the NiO diameter and the creation of O_2 vacancy [23]. The 5Ni15YZr was characterized by the lowest NiO crystal size and a high surface area.

Table 1. The textural features (surface properties) of the catalysts.

Catalyst	BET, m^2/g	Pore Volume, cm^3/g	Pore Diameter, nm	NiO Size *, nm
ZrO_2	21.0	0.160	37.0	
5Ni/Zr	16.0	0.150	42.0	31.60
5Ni/5YZr	27.0	0.230	31.0	15.80
5Ni/10YZr	23.0	0.190	25.0	15.40
5Ni/15YZr	25.0	0.180	24.0	13.80
5Ni/20YZr	24.0	0.170	22.0	16.40

* Crystalline size obtained via Debye–Scherrer method.

The hydrogen reduction temperature is an important standard for the catalytic oxidation properties of metal oxide support. H_2 -TPR measurements were adopted to identify the effects of the Y_2O_3 content on the reduction temperatures, and the profiles of all prepared catalysts are shown in Figure 2. The reduction temperature range may be classified into three zones—low, medium, and high—and each zone reflects the interaction and dispersion of the active metal with the support [24]. Mostly, all catalyst samples display a similar classification of bimodal at a medium temperature range, but with different patterns. Figure 2 shows the absence of peaks in the low zone (free NiO). The absence of free NiO species suggests that some interaction occurred between NiO and Y_2O_3 or ZrO_2 species. In addition, the weakly bound nickel species, such as nickel oxide (NiO), were easier to reduce but also more easily sintered, resulting in larger particles that promoted carbon formation. At 600 °C and above, there were no reduction peaks, denoting the absence of NiO species. In particular, 5NiZr had a distinctive reduction peak at 434°. On the other hand, adding the Y_2O_3 to the ZrO_2 significantly altered the range of the reduction temperature. Whenever the loading of Y_2O_3 was less than 10 wt.%, the synergy between the support and the active metal grew, consequently shifting the peaks to elevated temperatures. Conversely, if the Y_2O_3 loading exceeded 10 wt.%, synergy effects of the support and the active metal appeared at moderate temperatures. The temperature of Ni reduction varied with the different loading conditions of Y_2O_3 , which proves the differences in the activity and catalytic performance of each catalyst.

Because of the acidity of carbon dioxide, it is easily adsorbed on surfaces of basic sites. The basicity measurements of catalysts are essential for the regulation of carbon formation. The excessive basicity of the catalyst is detrimental to catalytic activity, as it stimulates a higher extent of CO_2 dissociation ($CO_2 \rightarrow C + O_2$), thus deactivating the catalyst. The phenomenon intensifies when the Boudouard reaction ($2CO \rightarrow C + CO_2$) starts to occur at high temperatures because of the enriched composition of CO upon methane reforming activity, thus resulting in a higher quantity of coke deposited on the catalyst's surface. The basicity of the prepared catalysts was characterized by CO_2 -TPD. Moreover, the CO_2 desorption peak area and temperature span regulate the basicity power. The feeble acid sites (surface hydroxyl) are physisorbed at 50–200 °C, while the medium-strength basic sites (surface oxygen anion) are chemisorbed at 200–400 °C, and the strong and very strong basic sites (bulk oxygen anion/oxygen vacancy) interact with oxygen vacancies at 400–650 °C and >650 °C, respectively [25,26]. The CO_2 -TPD profiles for all prepared catalysts are illustrated in Figure 3.

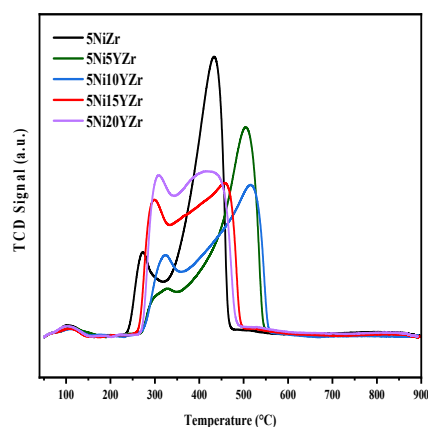


Figure 2. H₂-TPR profiles of the synthesized catalysts.

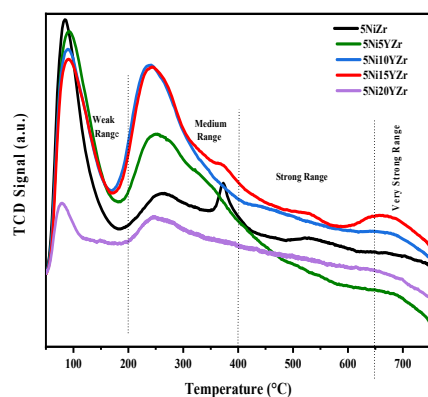


Figure 3. CO₂-TPD patterns of prepared catalysts.

The CO₂-TPD profiles show that all prepared catalysts presented the CO₂ desorption peaks in two major ranges: the first desorption peak, which occurred at lower temperatures of 50–200 °C (weak), and the second desorption peak, which occurred at higher temperatures of 200–400 °C (medium) because of the strength of the basic sites. An approximate highest temperature of 665 °C was recorded for the CO₂ desorption peaks in the very strong range with the exclusion of 5Ni15YZr and 5Ni10YZr. These desorption peaks are ascribed to strong basic sites [27]. Built on these outputs, the basicity sequence was as follows: 5Ni20YZr < 5NiZr < 5Ni5YZr < 5Ni10YZr < 5Ni15YZr. Catalytic basicity has a strong effect on the DRM reaction. However, there are other factors that influence catalytic performance, including surface area, pore size, active metal particle size, and dispersion [27]. Figure 4 shows the X-ray powder diffraction “XRPD” images of synthesized catalysts in 2θ = 10–80°. The XRPD image depicts the ZrO₂ phase. The images are similar, but the intensity decreased as the Y₂O₃ amount increased because of the reduction in the NiO diameter, and the Y₂O₃ peaks appeared clearly when their loading exceeded 10 wt.%. The peaks of low loading Y₂O₃ were not visible, as the particles of Y₂O₃ were incorporated into the pores of the zirconia. The diameter of the NiO is shown in Table 1. MDI Jade[®] software (version 6.5, Materials data Inc., Newtown Square, PA, USA) was used to inspect the diffraction data. The ZrO₂ monoclinic phase was identified at 24.170, 28.140, 31.470, 34.250, 38.580, 40.890, 44.870, 49.240, 54.000, 55.400, 57.250, 58.000, 60.000, 62.700, 65.000, 69.000, 71.300, 75.000, and 79.000° (JCPDS 81-1314) [28], whereas NiO diffraction peaks were identified at 35.340 and 45.500° (JCPDS 65-5745) [29]. The peaks of high loading Y₂O₃ were identified at 29.200, 31.000, and 50.200° (JCPDS 89-5592) [30]. The crystalline size calculations of 5NiZr, 5Ni5YZr, 5Ni10YZr, 5Ni15YZr, and 5Ni20YZr catalysts using the Debye–Scherrer method are tabulated in Table 1. The 5NiZr catalyst presented the highest NiO particle size and the lowest surface area, which negatively affected the activity and

stability performance, whereas the 5Ni15YZr catalysts with high surface area yielded the smallest NiO size and the best performance.

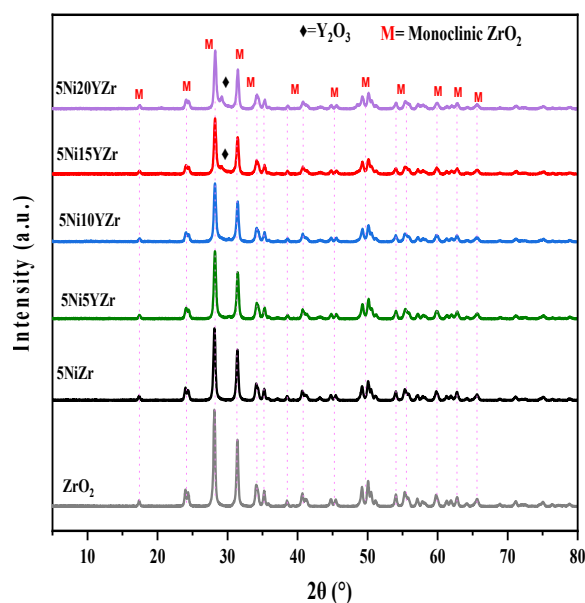


Figure 4. The XRPD patterns of synthesized catalysts.

Furthermore, the 5Ni15YZr catalyst had the highest conversion of methane and carbon dioxide when compared with the other prepared catalysts. It can be seen in Figure 5 that CH_4 and CO_2 conversion decreased in the order 5Ni15YZr > 5Ni10YZr > 5Ni5YZr > 5Ni20YZr > 5NiZr. Thus, on the basis of the catalytic performance of methane and carbon dioxide conversions and the different characterization methods of BET, TPR, CO_2 -TPD, XRPD, TAG, and TEM, it was shown that the 15 wt.% Y_2O_3 loading was optimal. Several studies [31–34] have investigated related systems in which the effect of the incorporation of alkaline earth and lanthanide metal oxides into the active metals, a process that develops oxygen vacancies, is observed. The blockage of the catalyst pores, feed flow, and inactivity results mainly from coke formation.

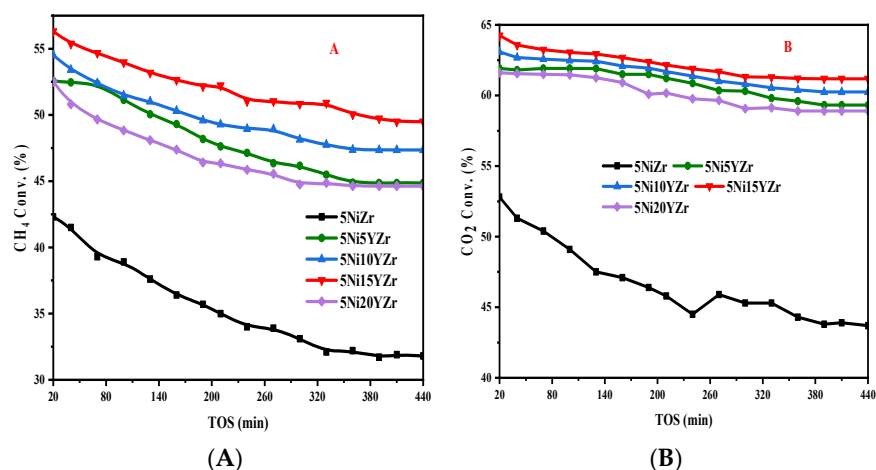


Figure 5. (A) CH_4 conversion %; (B) CO_2 conversion % versus time on stream at a reaction temperature of 700 °C.

Figure 6 shows the TGA analysis of the catalysts used. TGA was performed on the spent catalysts to determine the amount of carbon deposited on the catalysts. The weight loss below was caused by the removal of the deposited carbon. The weight drop began at

470 °C because of the burning of the coke, which inhibited the catalytic activity. The percent weight drop corresponded to the extent of the carbon formed. However, the addition of Y_2O_3 to 5NiZr for loading of less than 15.0 wt.% influenced the carbon deposition insignificantly. Alternatively, the 5Ni20YZr sample generated fair coke deposition. This could be related to the fact that the high loading of Y_2O_3 covers the active Ni catalyst excessively. Thus, the reactivity of the active Ni was lowered, and consequently, the amount of carbon deposited decreased. The weight % drop sequence was as follows: 5Ni20YZr < 5NiZr < 5Ni15YZr < 5Ni10YZr < 5Ni5YZr.

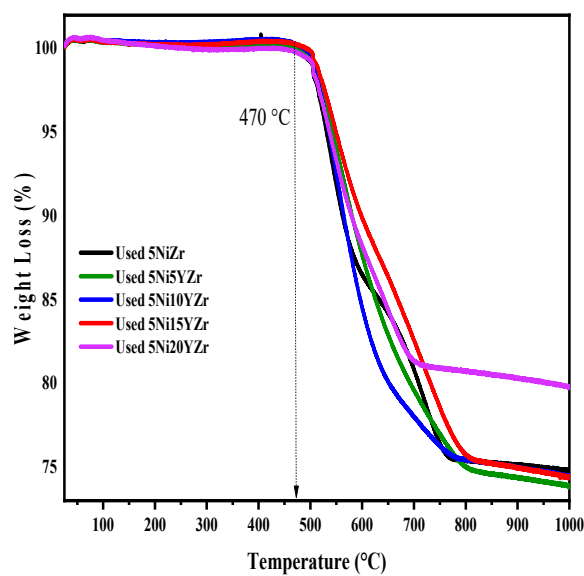


Figure 6. TGA profile for all spent catalysts at a reaction temperature of 700 °C.

The TEM for 5Ni15YZr was displayed to give a better visualization of the surface morphology and carbon deposition on the surface of the catalyst. The fresh sample had better distribution and a reduced active metal diameter. By contrast, the sample used showed slim sheets of multiwall carbon nanotubes. Figure 7 shows the TEM micrographs of the fresh and used samples of 5Ni15YZr.

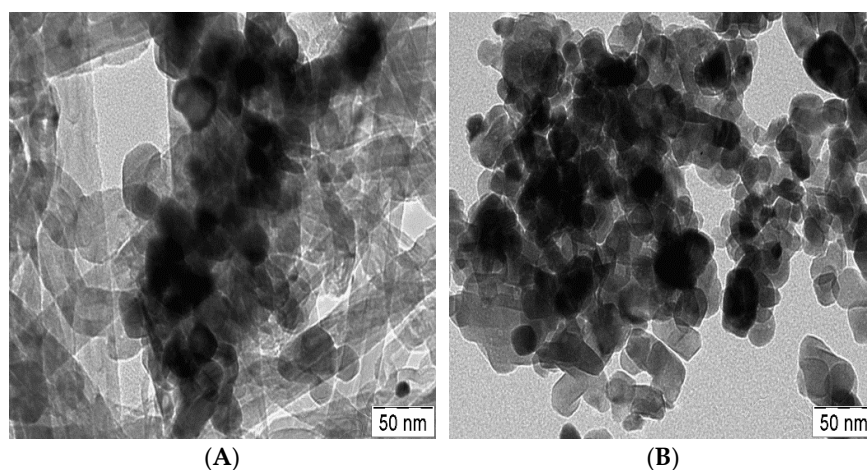


Figure 7. TEM micrographs for fresh (A) and used (B) 5Ni15YZr catalysts at a reaction temperature of 700 °C.

The performance of the 5Ni15YZr catalysts was further examined by combining the Ni with promoting elements, such as Cs, Ga, and Sr; 3 wt.% of the promoter was used. Figure 8 depicts the catalytic conversion of CH_4 and CO_2 against the time on stream. The

outcome showed that the first conversions of CH₄ and CO₂ for 5Ni15YZr, 5Ni153CsYZr, 5Ni3Ga15YZr, and 5Ni3Sr15YZr were 56.3%, 57.6%, 61.5%, and 66.5%, respectively, for CH₄ and 64.3%, 72.5%, 77.9%, and 79.7%, respectively, for CO₂. The Sr, Ga, and Cs promoters improved the percent conversion of CH₄ by 18%, 9%, and 2%, respectively, over the non-promoted 5Ni15YZr. This may be ascribed to the formation of alloyed structures with strongly modified electronic properties and the provision of extra active sites for reaction. Thus, the 5Ni3Sr15YZr catalyst outperformed the remaining catalysts and gave rise to the largest (66.5%) mean conversion of CH₄.

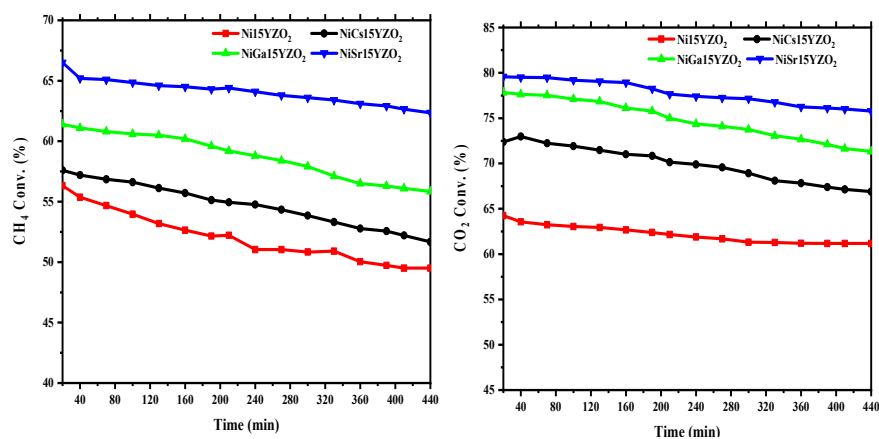


Figure 8. CH₄ and CO₂% conversions for 5Ni15YZr, 5NiCs15YZr, 5NiGa15YZr, and 5NiSr15YZr catalysts.

The thermogravimetric analysis of the used promoted catalysts obtained after 440 min of reaction was carried out. Figure 9 exhibits the percent weight loss profiles. The percent weight loss is in accordance with the type of promoter. Thus, the 5Ni15SrYZr catalyst produces 9.7% weight loss, which is the highest value, while the 5Ni15CsYZr catalyst generated a minimum weight loss of 2.6% as a result of carbon deposition. For the promoted catalysts, the higher the activity of the sample, the greater the amount of carbon formed, which was in line with the scale of the reaction. The promoted samples displayed slight carbon formation in contrast to the non-promoted sample (5Ni15YZr), providing a 25.60% weight drop. The promoted catalysts formed stable ZrO₂ phases and additional mixed phases of cubic zirconium promoter oxide. Therefore, promoters enhanced the stability of the catalyst. This could be associated with the fact that the elevated loading of Y₂O₃ covered the active Ni catalyst excessively. Thus, the reactivity of the active Ni was lowered, and consequently, the amount of carbon deposited decreased. The percent weight drop sequence of the catalysts was as follows: 5Ni20YZr < 5NiZr < 5Ni15YZr < 5Ni10YZr < 5Ni5YZr.

Figure 10 shows the TEM micrographs of the fresh and used samples of the promoted 5Ni15YZr at 100 nm magnification. For a wider comprehension of carbon formation and structure, the TEM of the promoted catalysts was typically carried out to elucidate the surface structure and carbon deposition on the surface of the catalyst. The fresh samples of the promoted catalysts (A, B, and C) had better scatter and insignificant active metal diameters. By contrast, the promoted samples used (a', b', and c') exhibited accumulated particles over the surface and formation of the carbon nanotubes.

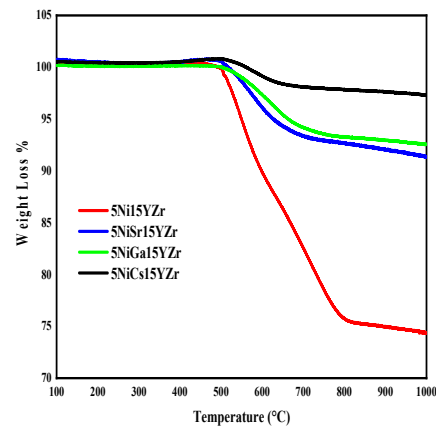


Figure 9. TGA plot for promoted used catalysts at 700 °C after 440 min.

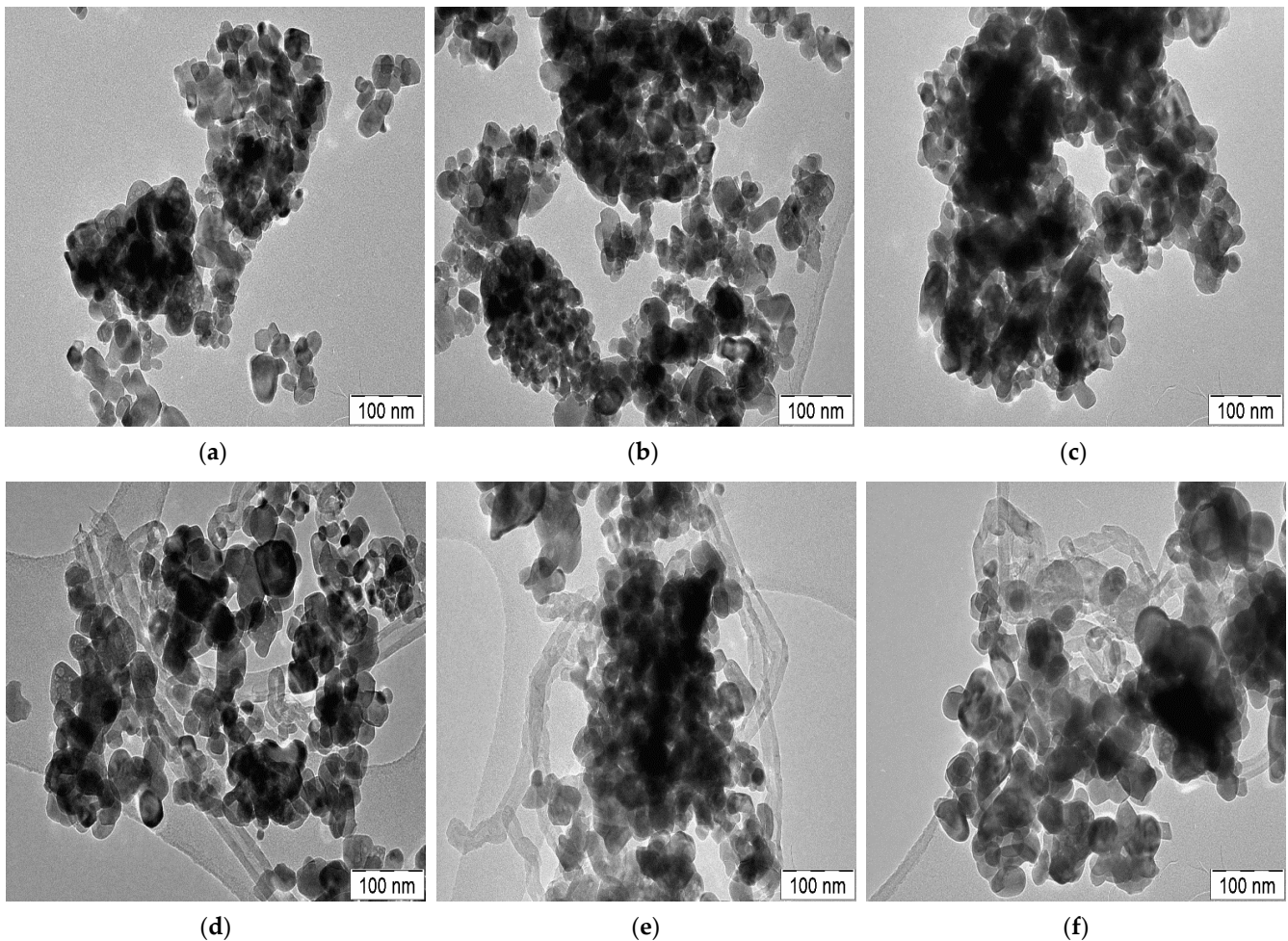


Figure 10. TEM micrographs for fresh (a) Sr, (b) Ga, and (c) Cs and used (d) Sr, (e) Ga, and (f) Cs promoted 5Ni15YZr catalysts at a reaction temperature of 700 °C.

Figure 11 shows the Raman spectra of the promoted catalysts used. The addition of the promoter altered the structure of the pristine catalyst 5Ni15YZr because the promoter incorporation resulted in the formation of stable ZrO_2 phases and other mixed phases of cubic zirconium promoter oxide. The promoted catalysts displayed three bands with Raman shifts of 816–857 cm^{-1} , 966–979 cm^{-1} and 1112–1115 cm^{-1} for the 5NiGa15YZr and 5NiCs15YZr catalysts, which shifted to lower values of 654.0 cm^{-1} , 885.0 cm^{-1} , and 1006.0 cm^{-1} for NiSr15YZr catalyst. 5Ni15YZr showed a similar peak at 612.0 cm^{-1} . The

peaks for the promoted samples could be associated with the instigated disorders in the graphite (d), the ideal vibration of the graphite layers (g), and the overtone of the d band (d1) [35]. Commonly, the ratio intensities of the d and g bands denote the amount of graphite relative to carbonaceous materials [36]. The recorded fractions were 0.840, 0.880, and 0.740 for 5NiGa15YZr, 5NiCs15YZr, and 5NiSr15YZr, respectively, denoting a dominance of graphitization as the ratios are less than unity. The best catalyst, 5NiSr15YZr, presented the lowest ratio.

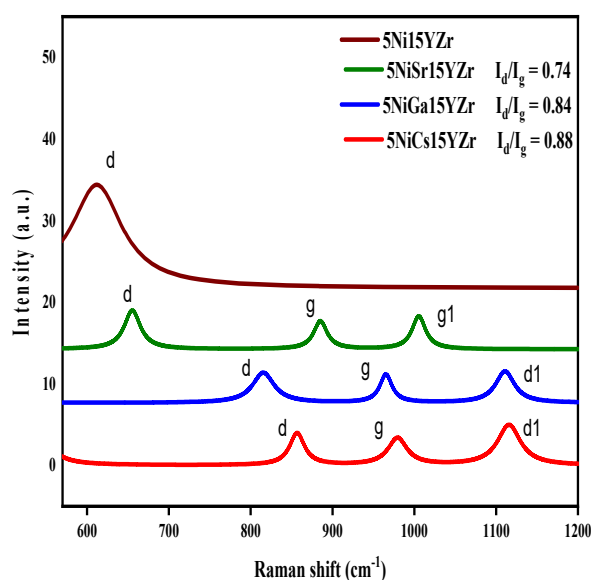


Figure 11. Raman spectra for the promoted spent catalysts.

The catalysts 5Ni15YZr and 5NiSr15YZr gave the best results among all catalysts for the non-promoted and promoted catalysts, respectively. As a result, these catalysts became targets for further investigation in a sensitivity analysis. Typically, in sensitivity analysis experiments, the effects of the flow rate and reaction temperature are studied. Figure 12 presents the effect of the reaction temperature on the CH₄ and CO₂ conversions of both 5Ni15YZr and 5NiSr15YZr catalysts. As expected, the reaction temperature was directly proportional to the conversion of reactants owing to the highly endothermic feature of the DRM reaction. The effect of reaction temperatures of 500–650 °C was very weak, but the effect was strong and clear when the temperature reached 700 °C; there was a small difference between the reaction temperature results of 700 °C and 750 °C, and the highest effect of the reaction temperature was obtained at 800 °C.

Figure 13 shows the effects of two different flow rates on the CH₄ and CO₂ conversions of both the 5Ni15YZr and 5NiSr15YZr catalysts. The lower flow rate provided better activity performances of CH₄ and CO₂. This could be related to the fact that the low flow rate causes a longer residence time of the reactants on the catalyst. Figure 13 also shows that the 5NiSr15YZr catalyst maintained better performance than the 5Ni15YZr catalyst for the different flow rates.

Figure 14 displays the TGA analysis of the spent 5Ni15YZr catalyst at different (CH₄/CO) feed flow rates. The percent weight loss for the lower feed flow rate was higher, as expected, because of the high conversion of the reactant and the long interaction time between the feed and the catalyst.

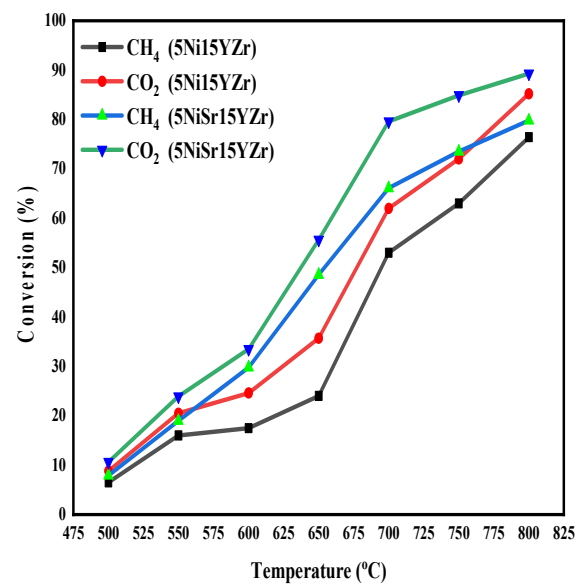


Figure 12. Conversion versus reaction temperature for 5Ni15YZr and 5NiSr15YZr.

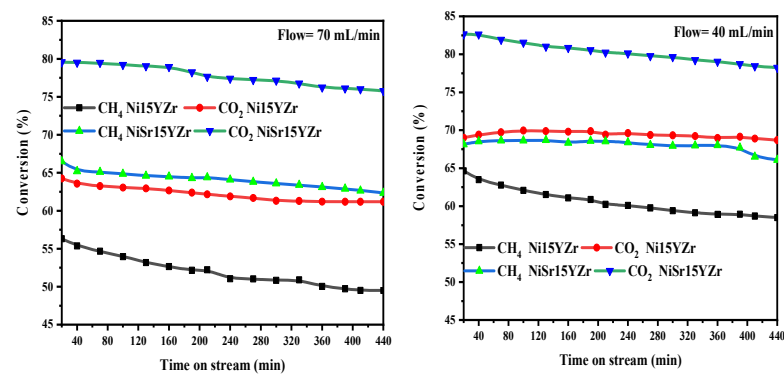


Figure 13. Conversion versus time on stream for 5Ni15YZr and 5NiSr15YZr at different feed flow rates.

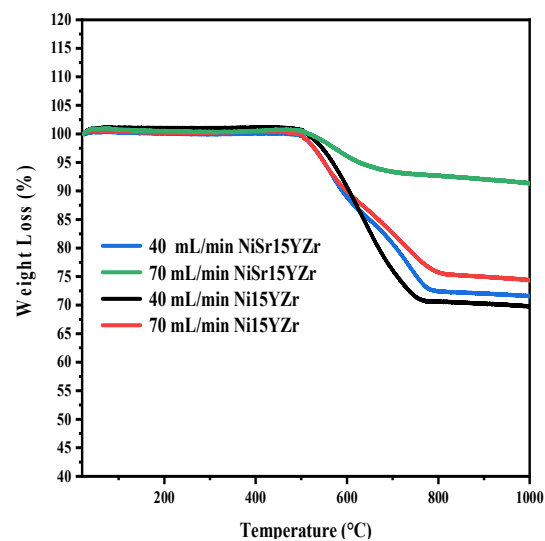


Figure 14. TGA profile for used 5Ni15YZr and 5NiSr15YZr at different reactant flow rates.

The addition of Y_2O_3 up to 15 wt.% was found to enhance the basicity and optimize the Ni size (13.8 nm). High basicity induced improved CO_2 interaction, whereas size-

optimized Ni conveyed controlled CH₄ dissociation. Controlled CH₄ dissociation and sequential carbon deposit oxidation by CO₂ over the 5Ni15YZr catalyst system led to the highest catalytic activity (>50% CH₄ conversion and >60% CO₂ conversion) toward dry reforming of methane. Furthermore, the addition of the alkaline earth metal Sr may have induced additional basicity over the surface. In our previous research, Sr addition was found to upgrade the basicity of the catalyst [37,38], which may induce additional CO₂ adsorption over the catalyst's surface. The reactions of Sr(OH)₂ with CO₂ and SrH₂ with CO₂ have already been established [39,40], and the increased interaction of CO₂ over an Sr-modified surface can be accepted. Overall, 15 wt.% Y and 15 wt.% Sr addition over the zirconia-supported Ni catalyst induced proper basicity, which is needed for optimal catalytic performance and minimal coke deposition at a 70 mL/min CH₄: CO₂ flow rate

4. Conclusions

The performance of DRM was investigated in a micro-tubular fixed-bed reactor. Various characterization techniques, such as the N₂-physisorption analyzer, temperature-programmed techniques, TGA, XRPD, and TEM, were implemented. The textural properties of the catalysts using the N₂-physisorption analyzer showed low specific surface areas, which were reflected by their low specific volume of adsorbed nitrogen gas, lying in the range of 4.5–8.0 cm³/g. The BET surface area of the catalysts increased when Y₂O₃ was added. The TPR analysis depicted that all samples had the same classification, which was bimodal at the intermediate temperature where the metal support interaction was neither weak nor strong. The addition of Y₂O₃ had a positive effect, as it lowered the temperature of reduction. The CO₂-TPD profiles showed that all prepared catalysts presented CO₂ desorption peaks at 50–200 °C and 200–400 °C, ascribable to low and medium basic strength sites. The basicity of the catalysts increased significantly with the Y₂O₃ loading. The morphology of the used catalyst via TEM showed that the carbon formed was in the form of nano-filaments containing multi-walled carbon nanotubes. The promotion of 5Ni15YZr with Cs, Ga, and Sr enhanced the average methane conversion by 2, 9, and 18%, respectively. The flow rate and reaction temperature sensitivity analysis of the best catalysts (5Ni15YZr and 5NiSr15YZr) exhibited that the lower the flow of the reactants, the higher the activity, and vice versa. The catalytic performance increased with an increase in the reaction temperature from 500 to 800 °C. The TGA analysis revealed lower carbon formation for Sr-promoted catalysts. The purpose of this paper was achieved. The Y₂O₃ modifier enhanced the performance of the pristine support, and the best loading was attained. Moreover, Sr was revealed to be the optimum promoter; it raised the activity, and, together with Y, low carbon deposition was recorded.

Supplementary Materials: The following supporting information can be downloaded at: <https://www.mdpi.com/article/10.3390/en15103841/s1>, Figure S1: EDX image of fresh 5Ni10YZr catalyst; Table S1: Catalysts and their Designations.

Author Contributions: A.A.I., A.S.A.-F. and A.K.: conceptualization, data curation, and writing—original draft preparation. Y.A.A.-B.: characterization tests and writing parts of the manuscript. A.E.A., A.S.A.-F. and A.H.F.: writing—review and editing, supervision, project administration, contribution to the analysis of the data, and proofreading of the manuscript. All authors have read and agreed to the published version of the manuscript.

Funding: This research was funded by Researchers Supporting Project number (RSP-2021/368), King Saud University, Riyadh, Saudi Arabia.

Acknowledgments: The authors would like to extend their sincere appreciation to Researchers Supporting Project number (RSP-2021/368), King Saud University, Riyadh, Saudi Arabia.

Conflicts of Interest: There are no conflict of interest to declare.

References

1. Boaro, M.; Colussi, S.; Trovarelli, A. Ceria-based materials in hydrogenation and reforming reactions for CO₂ valorization. *Front. Chem.* **2019**, *7*, 28. [[CrossRef](#)] [[PubMed](#)]
2. Al-Fatesh, A.S.; Arafat, Y.; Ibrahim, A.A.; Atia, H.; Fakeeha, A.H.; Armbruster, U.; Abasaheed, A.E.; Frusteri, F. Evaluation of Co-Ni/Sc-SBA-15 as a novel coke resistant catalyst for syngas production via CO₂ reforming of methane. *Appl. Catal. A Gen.* **2018**, *567*, 102–111. [[CrossRef](#)]
3. Danghyan, V.; Kumar, A.; Mukasyan, A.; Wolf, E.E. An active and stable NiOMgO solid solution based catalysts prepared by paper assisted combustion synthesis for the dry reforming of methane. *Appl. Catal. B Environ.* **2020**, *273*. [[CrossRef](#)]
4. Marinho, A.L.A.; Rabelo-Neto, R.C.; Epron, F.; Bion, N.; Toniolo, F.S.; Noronha, F.B. Embedded Ni nanoparticles in CeZrO₂ as stable catalyst for dry reforming of methane. *Appl. Catal. B Environ.* **2020**, *268*, 118387. [[CrossRef](#)]
5. Dou, J.; Zhang, R.; Hao, X.; Bao, Z.; Wu, T.; Wang, B.; Yu, F. Sandwiched SiO₂@Ni@ZrO₂ as a coke resistant nanocatalyst for dry reforming of methane. *Appl. Catal. B Environ.* **2019**, *254*, 612–623. [[CrossRef](#)]
6. Khani, Y.; Shariatnia, Z.; Bahadoran, F. *High Catalytic Activity and Stability of ZnLaAlO₄ Supported Ni, Pt and Ru Nanocatalysts Applied in the Dry, Steam and Combined Dry-Steam Reforming of Methane*; Elsevier: Amsterdam, The Netherlands, 2016.
7. Niu, J.; Du, X.; Ran, J.; Wang, R. *Dry (CO₂) Reforming of Methane over Pt Catalysts Studied by DFT and Kinetic Modeling*; Elsevier: Amsterdam, The Netherlands, 2016.
8. Mourhly, A.; Kacimi, M.; Halim, M.; Arsalane, S. New low cost mesoporous silica (MSN) as a promising support of Ni-catalysts for high-hydrogen generation via dry reforming of methane (DRM). *Int. J. Hydrogen Energy* **2020**, *45*, 11449–11459. [[CrossRef](#)]
9. Arif, N.N.M.; Vo, D.-V.N.; Azizan, M.T.; Abidin, S.Z. Carbon dioxide dry reforming of glycerol for hydrogen production using Ni/ZrO₂ and Ni/CaO as catalysts. *Bull. Chem. React. Eng. Catal.* **2016**, *11*, 200–209. [[CrossRef](#)]
10. Chen, L.; Qi, Z.; Zhang, S.; Su, J.; Somorjai, G.A. Catalytic Hydrogen Production from Methane: A Review on Recent Progress and Prospect. *Catalysts* **2020**, *10*, 858. [[CrossRef](#)]
11. Vogt, C.; Kranenborg, J.; Monai, M.; Weckhuysen, B.M. Structure sensitivity in steam and dry methane reforming over nickel: Activity and carbon formation. *ACS Catal.* **2019**, *10*, 1428–1438. [[CrossRef](#)]
12. Zuo, Z.; Liu, S.; Wang, Z.; Liu, C.; Huang, W.; Huang, J.; Liu, P. Dry Reforming of Methane on Single-Site Ni/MgO Catalysts: Importance of Site Confinement. *ACS Catal.* **2018**, *8*, 9821–9835. [[CrossRef](#)]
13. Al-Fatesh, A.; Fakeeha, A.; Aidid, A.; Abasaheed, I.-E. *Ni Supported on La₂O₃ + ZrO₂ for Dry Reforming of Methane: The Impact of Surface Adsorbed Oxygen Species*; Elsevier: Amsterdam, The Netherlands, 2021.
14. Harrison, D.P. Sorption-enhanced hydrogen production: A review. *Ind. Eng. Chem. Res.* **2008**, *47*, 6486–6501. [[CrossRef](#)]
15. Wysocka, I.; Mielewczyk-Gryń, A.; Łapiński, M.; Cieślík, B.; Rogala, A. Effect of small quantities of potassium promoter and steam on the catalytic properties of nickel catalysts in dry/combined methane reforming. *Int. J. Hydrogen Energy* **2021**, *46*, 3847–3864. [[CrossRef](#)]
16. Azeanni, N.; Ghani, A.; Azapour, A.; Faua'ad, A.; Muhammad, S.; Abdullah, B. Dry reforming of methane for hydrogen production over NiCo catalysts: Effect of NbeZr promoters. *Int. J. Hydrogen Energy* **2018**. [[CrossRef](#)]
17. Wang, S.F.; Zhang, J.; Luo, D.W.; Gu, F.; Tang, D.Y.; Dong, Z.L.; Tan, G.E.B.; Que, W.X.; Zhang, T.S.; Li, S. Transparent ceramics: Processing, materials and applications. *Prog. Solid State Chem.* **2013**, *41*, 20–54. [[CrossRef](#)]
18. Bellido, J.D.A.; Assaf, E.M. Effect of the Y₂O₃-ZrO₂ support composition on nickel catalyst evaluated in dry reforming of methane. *Appl. Catal. A Gen.* **2009**, *352*, 179–187. [[CrossRef](#)]
19. Bellido, J.D.A.; Assaf, E.M. Nickel catalysts supported on ZrO₂, Y₂O₃-stabilized ZrO₂ and CaO-stabilized ZrO₂ for the steam reforming of ethanol: Effect of the support and nickel load. *J. Power Sources* **2008**, *177*, 24–32. [[CrossRef](#)]
20. Rezaee, S.; Rashed, G.R.; Golozar, M.A. Electrochemical and oxidation behavior of yttria stabilized zirconia coating on zircaloy-4 synthesized via sol-gel process. *Int. J. Corros.* **2013**, *2013*, 453835. [[CrossRef](#)]
21. Oliveira, D.M.; Andrada, A.S. Synthesis of ordered mesoporous silica MCM-41 with controlled morphology for potential application in controlled drug delivery systems. *Cerâmica* **2019**, *65*, 170–179. [[CrossRef](#)]
22. Brockner, W.; Ehrhardt, C.; Gjikaj, M. Thermal decomposition of nickel nitrate hexahydrate, Ni(NO₃)₂·6H₂O, in comparison to Co(NO₃)₂·6H₂O and Ca(NO₃)₂·4H₂O. *Thermochim. Acta* **2007**, *456*, 64–68. [[CrossRef](#)]
23. Marcos, P.J.B.; Gouvêa, D. Effect of MgO segregation and solubilization on the morphology of ZrO₂ powders during synthesis by the Pechini's method. *Cerâmica* **2004**, *50*, 38–42. [[CrossRef](#)]
24. Sadeq Al-Fatesh, A.; Olajide Kasim, S.; Aidid Ibrahim, A.; Hamza Fakeeha, A.; Elhag Abasaheed, A.; Alrasheed, R.; Ashamari, R.; Bagabas, A. Combined magnesia, ceria and nickel catalyst supported over γ-alumina doped with titania for dry reforming of methane. *Catalysts* **2019**, *9*, 188. [[CrossRef](#)]
25. Al-Fatesh, A.S.; Naeem, M.A.; Fakeeha, A.H.; Abasaheed, A.E. CO₂ reforming of methane to produce syngas over γ-Al₂O₃-supported Ni-Sr catalysts. *Bull. Chem. Soc. Jpn.* **2013**, *86*, 742–748. [[CrossRef](#)]
26. Naeem, M.A.; Al-Fatesh, A.S.; Abasaheed, A.E.; Fakeeha, A.H. Activities of Ni-based nano catalysts for CO₂-CH₄ reforming prepared by polyol process. *Fuel Process. Technol.* **2014**, *122*, 141–152. [[CrossRef](#)]
27. Fakeeha, A.H.; Al Fatesh, A.S.; Ibrahim, A.A.; Kurdi, A.N.; Abasaheed, A.E. Yttria Modified ZrO₂ Supported Ni Catalysts for CO₂ Reforming of Methane: The Role of Ce Promoter. *ACS Omega* **2021**, *6*, 1280–1288. [[CrossRef](#)]
28. Rauta, P.R.; Manivasakan, P.; Rajendran, V.; Sahu, B.B.; Panda, B.K.; Mohapatra, P. Phase transformation of ZrO₂ nanoparticles produced from zircon. *Phase Transit.* **2012**, *85*, 13–26. [[CrossRef](#)]

29. Lu, H.; Zheng, M.; Chen, J.; Li, N.; Xue, L.; Cao, J. An Easy and Green Route for the Fabrication of NiO Nanoparticles by Starch Template. *Integr. Ferroelectr.* **2011**, *127*, 128–133. [[CrossRef](#)]
30. Jung, H.-Y.; Kim, H.-J.; Yang, S.; Kang, Y.-G.; Oh, B.-Y.; Park, H.-G.; Seo, D.-S. Enhanced electro-optical properties of Y₂O₃ (yttrium trioxide) nanoparticle-doped twisted nematic liquid crystal devices. *Liq. Cryst.* **2012**, *39*, 789–793. [[CrossRef](#)]
31. Dow, W.-P.; Wang, Y.-P.; Huang, T.-J. TPR and XRD studies of yttria-doped ceria/ γ -alumina-supported copper oxide catalyst. *Appl. Catal. A Gen.* **2000**, *190*, 25–34. [[CrossRef](#)]
32. Dow, W.-P.; Huang, T.-J. Yttria-stabilized zirconia supported copper oxide catalyst: II. Effect of oxygen vacancy of support on catalytic activity for CO oxidation. *J. Catal.* **1996**, *160*, 171–182. [[CrossRef](#)]
33. Kawamura, K.; Watanabe, K.; Hiramatsu, T.; Kaimai, A.; Nigara, Y.; Kawada, T.; Mizusaki, J. Electrical conductivities of CaO doped ZrO₂–CeO₂ solid solution system. *Solid State Ion.* **2001**, *144*, 11–18. [[CrossRef](#)]
34. Wang, J.B.; Tai, Y.-L.; Dow, W.-P.; Huang, T.-J. Study of ceria-supported nickel catalyst and effect of yttria doping on carbon dioxide reforming of methane. *Appl. Catal. A Gen.* **2001**, *218*, 69–79. [[CrossRef](#)]
35. Reich, S.; Thomsen, C. Raman spectroscopy of graphite. *R. Soc.* **2004**, *362*, 2271–2288. [[CrossRef](#)] [[PubMed](#)]
36. Kameya, Y.; Hanamura, K. Kinetic and Raman spectroscopic study on catalytic characteristics of carbon blacks in methane decomposition. *Chem. Eng. J.* **2011**, *173*, 627–635. [[CrossRef](#)]
37. Ibrahim, A.A.; Fakeeha, A.H.; Al-Fatesh, A.S. Enhancing hydrogen production by dry reforming process with strontium promoter. *Int. J. Hydrogen Energy* **2014**, *39*, 1680–1687. [[CrossRef](#)]
38. Al-Fatesh, A. Suppression of carbon formation in CH₄–CO₂ reforming by addition of Sr into bimetallic Ni–Co/ γ -Al₂O₃ catalyst. *J. King Saud Univ. Eng. Sci.* **2015**, *27*, 101–107. [[CrossRef](#)]
39. Li, Q.; Xu, B.; Huang, T.; Yu, W.; Wang, X. Activation of CO₂ by Alkaline-Earth Metal Hydrides: Matrix Infrared Spectra and DFT Calculations of HM(O₂CH) and (MH₂)(HCOOH) Complexes (M = Sr, Ba). *Inorg. Chem.* **2021**, *60*, 11466–11473. [[CrossRef](#)]
40. Li, S.; Zhang, H.; Xu, J.; Yang, D. Hydrothermal synthesis of flower-like SrCO₃ nanostructures. *Mater. Lett.* **2005**, *59*, 420–422. [[CrossRef](#)]